


Hyaluronic Acid-Bilirubin Nanoparticles as a Tumor Microenvironment Reactive Oxygen Species-Responsive Nanomedicine for Targeted Cancer Therapy

Seonju Lee, Seon Ah Lee, Jongyoon Shinn, Yonghyun Lee 

College of Pharmacy, Ewha Womans University, Seoul, 03760, South Korea

Correspondence: Yonghyun Lee, College of Pharmacy, Ewha Womans University, Seoul, 03760, South Korea, Email y.lee@ewha.ac.kr

Introduction: The tumor microenvironment (TME) has attracted considerable attention as a potential therapeutic target for cancer. High levels of reactive oxygen species (ROS) in the TME may act as a stimulus for drug release. In this study, we have developed ROS-responsive hyaluronic acid-bilirubin nanoparticles (HABN) loaded with doxorubicin (DOX@HABN) for the specific delivery and release of DOX in tumor tissue. The hyaluronic acid shell of the nanoparticles acts as an active targeting ligand that can specifically bind to CD44-overexpressing tumors. The bilirubin core has intrinsic anti-cancer activity and ROS-responsive solubility change properties.

Methods & Results: DOX@HABN showed the HA shell-mediated targeting ability, ROS-responsive disruption leading to ROS-mediated drug release, and synergistic anti-cancer activity against ROS-overproducing CD44-overexpressing HeLa cells. Additionally, intravenously administered HABN-Cy5.5 showed remarkable tumor-targeting ability in HeLa tumor-bearing mice with limited distribution in major organs. Finally, intravenous injection of DOX@HABN into HeLa tumor-bearing mice showed synergistic anti-tumor efficacy without noticeable side effects.

Conclusion: These findings suggest that DOX@HABN has significant potential as a cancer-targeting and TME ROS-responsive nanomedicine for targeted cancer treatment.

Keywords: tumor microenvironment, reactive oxygen species, hyaluronic acid-bilirubin nanomedicine, stimuli-responsive nanomedicine

Introduction

The tumor microenvironment (TME) can serve as a “soil” with conditions that are conducive to providing growth, survival, and metastasis of tumor cells or “seeds”. Thus, the TME has a crucial role in the survival and treatment of patients with tumors.^{1–3} The characteristics of the TME differ from normal tissue, such as hypoxia, mildly acidic pH, high levels of reactive oxygen species (ROS), and elevated levels of certain enzymes.^{2,4–9} Among these features, the high levels of ROS generated by cancer cells and TME-associated cells such as cancer-associated fibroblasts, myeloid-derived suppressor cells, and tumor-associated macrophages have received significant attention as a stimulus for efficient drug release from ROS-responsive nanomedicines.^{10–15} Although various ROS-responsive nanoparticles have been developed, most have drawbacks such as *de novo*-synthesized artificial material-based potential toxicity issues, slow ROS responsiveness, and/or complexity of final nano-formulations, limiting their clinical translation.^{15–17} Therefore, there is a need for biocompatible ROS-responsive nanoparticles that can act rapidly with a simple formulation.^{15,18}

A combination of two or more anti-cancer therapeutics is a general approach in most cancer regimens. However, combining multiple anti-cancer therapeutics in a single nanoparticle increases the complexity of the nanoformulation,

hindering clinical translation.^{19–21} Thus, the intrinsic anti-cancer activity of a nanoparticle itself could enhance the synergistic anti-cancer activity of an encapsulated anti-cancer agent, reducing the complexity of the formulation.^{22,23}

Toward this goal, we used hyaluronic acid-bilirubin nanoparticles (HABN), which are biocompatible and versatile nanoparticles with a simple formulation. The bilirubin (BR) core endows HABN with two key features: 1) rapid responsiveness to ROS facilitated by the solubility changes of the hydrophobic BR core to hydrophilic biliverdin and BR oxidative products, and 2) intrinsic therapeutic efficacy attributed to the anti-cancer activity of the BR core.^{24–26} Moreover, due to the CD44-targeting capacity of the hydrophilic hyaluronic acid (HA) shell, HABN has the potential to target cells that overexpress CD44.^{27–30} Our previous reports have highlighted the compelling features of HABN,^{27,31,32} such as gut microbiome modulation activity, intrinsic therapeutic potential against colitis, and ability to target CD44-overexpressing cells such as macrophages, tumor cells, activated hepatic stellate cells, and intestinal epithelial cells. However, the potential impact of HABN in targeting ROS-overproducing and CD44-overexpressing tumors while simultaneously demonstrating ROS-mediated drug release and intrinsic therapeutic efficacy remains unexplored. Notably, although PEGylated BR nanoparticles rely on extra components for active targeting, HABN demonstrates active targeting itself without the need for any additional components, simplifying the system significantly.^{27,31,33,34}

Thus, we present findings on doxorubicin (DOX)-loaded HABN (DOX@HABN) designed to target the elevated oxidative stress within the TME of CD44-overexpressing tumors, resulting in enhanced anti-tumor activity (Figure 1). In this study, we emphasize the remarkably strong tumor-targeting ability of HABN, which is probably due to the intrinsic TME ROS and CD44-targeting ability of HABN against HeLa tumors (cervical adenocarcinoma) overexpressing CD44 and overproducing ROS. Furthermore, we demonstrate the synergistic therapeutic potential of DOX@HABN against HeLa tumors. Overall, our findings suggest that DOX@HABN is a promising TME-targeted cancer therapy that has the potential to enhance anti-tumor potency and efficacy by releasing drugs that penetrate deep into tumors and eventually into cancer cells.

Materials and Methods

Synthesis of the Hyaluronic Acid-Bilirubin Conjugate (HA-BR)

The HA-BR conjugate was prepared from an acid form of HA (Lifecore Biomedical) and an amino-ethylene-bilirubin conjugate (AE-BR) using a slightly modified method based on the one previously described by Lee et al^{27,31} In brief, 80 μmol of the acidic form of HA, prepared from an HA sodium salt (Lifecore Biomedical) using a dialysis method, and 40 μmol of NHS were mixed in 4.8 mL of DMSO. After adding 140 μmol of EDC, the mixture was stirred for 10 min at RT. Then, 20 μmol of AE-BR, prepared from BR and ethylenediamine using a simple EDC chemistry, were added to the mixture. Subsequently, the mixture was stirred overnight at RT under nitrogen gas. Dialysis was carried out against 0.01 M NaOH 6 times for 20 h, water/acetonitrile (1:1) for 3 h, and then distilled water twice for 3 h. Finally, HA-BR (native sodium salt form; 26.5 $\mu\text{g}/\text{mL}$ of BR in 1 mg/mL of HABNs) was obtained through lyophilization. ¹H NMR spectra were obtained on an ANANCE Neo 400MHz system (Bruker); chemical shifts represent ppm downfield from tetramethylsilane. The BR portion of the HABNs was calculated using UV/VIS spectra from an Elisa reader (Multiskan GO with Cuvette function, Thermo Fisher Scientific).

Synthesis of PEGylated Bilirubin (PEG-BR)

PEG-BR was prepared as described previously with modifications.³³ Briefly, 75 μmol of BR and 33.75 μmol of EDC were added to 0.6 mL of DMSO containing 225 μL of trimethylamine and 52 μmol of NHS for 10 min at RT. Then, 15 μmol of polyethylene glycol 20 K-amine (PEG-NH₂, Nanocs) was added, and the mixture was stirred for 4 h under nitrogen gas. Subsequently, the mixture was added to 50 mL of chloroform, and the organic solvents were washed with 50 mL of 0.1 M HCl twice, followed by a wash with 50 mL of 0.1 M NaHCO₃ twice and finally with 50 mL of DW twice. The organic layer was evaporated, and 50 mL of methanol was added to the residue. After centrifugation at 3000g for 10 min, the supernatant was collected and evaporated. Dialysis was performed as described in the previous section. To yield PEG-BR, lyophilization was performed.

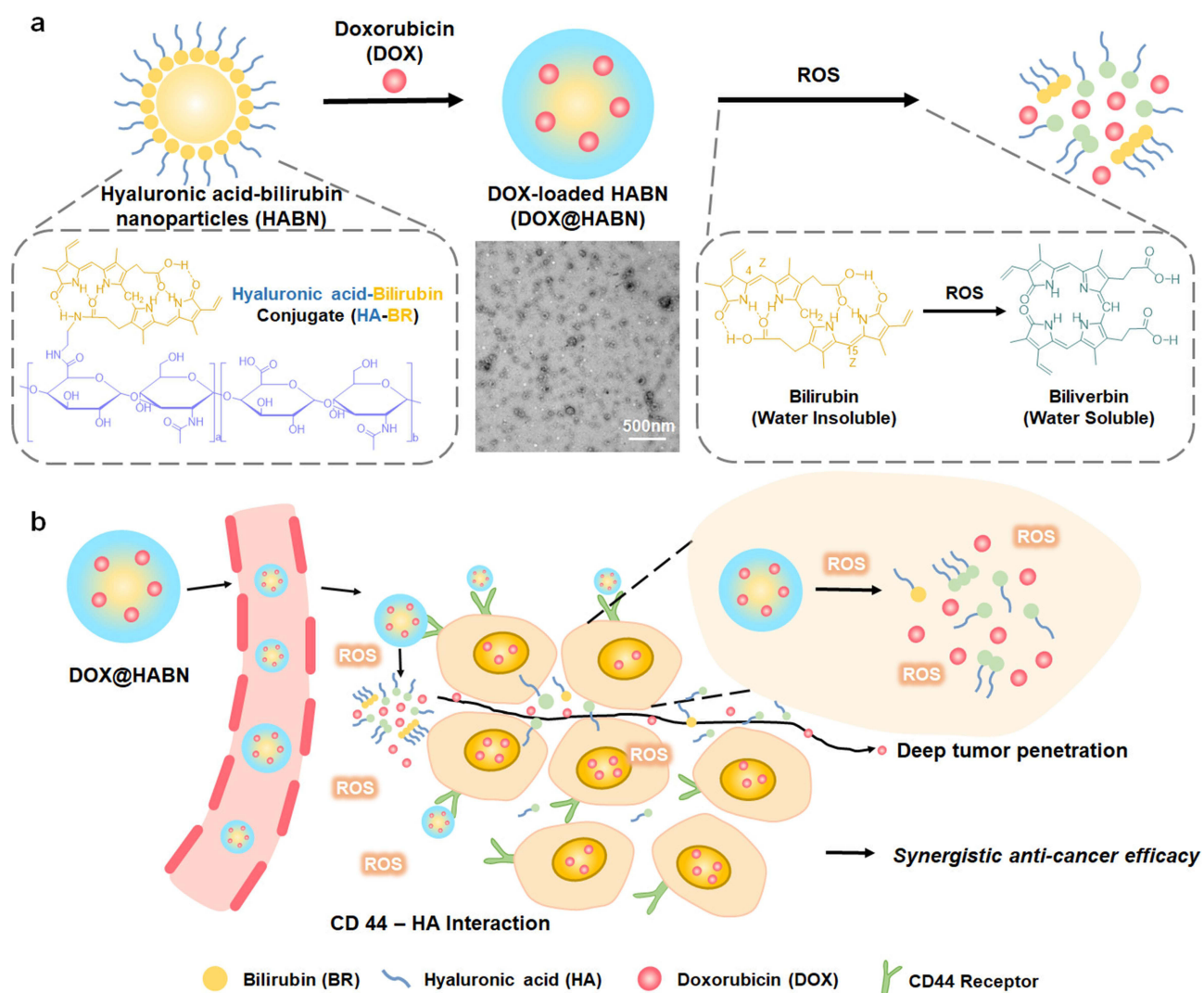


Figure 1 Doxorubicin-loaded hyaluronic acid-bilirubin nanoparticles (DOX@HABN) show therapeutic potential in CD44-positive/ROS-overproducing HeLa tumors. (a) Schematic of DOX@HABN self-assembled from HA-BR and DOX and a TEM image. Scale bar, 500 nm. (b) DOX@HABN could target CD44 on the HeLa tumor. In the tumor microenvironment and intracellular region, DOX@HABN is rapidly disassembled, releasing DOX that penetrates and diffuses deep into the tumor and ultimately into cancer cells.

Synthesis of HABN-Cy5.5

To acquire an acidic form of HABN, dialysis was performed against 0.1 M HCl overnight, followed by lyophilization. Then, 4 mg of the acidic form of HA-BR was dissolved in 0.8 mL of DMSO overnight, and 2 μmol of NHS and 2 μmol of EDC were added to the mixture. After mixing for 10 min at RT, 0.1 μmol of Cy5.5-NH₂ (AAT Bioquest) was added to the reaction mixture. After stirring overnight at RT, dialysis was performed against 0.01 M HCl for one day. Finally, HABN-Cy5.5 was acquired after lyophilization.

Preparation of DOX-Loaded HABN (DOX@HABN)

Before preparing DOX-loaded HABN (DOX@HABN), 0.5 mg of DOX HCl salt (Ark Pharm) was added to 1 mL of chloroform containing 5.7 μmol (0.5 μL) of triethylamine (TEA, Sigma Aldrich), and then the mixture was stirred at RT overnight. After washing with 1 mL of water 5 times, hydrophobic DOX was acquired via oven drying. DOX@HABN was easily prepared using the film layer method. Briefly, 0.5 or 4 mg of DOX and 1 or 4 mg of HA-BR were added to 1 or 4 mL of chloroform, respectively; mixed for 5 min; and then chloroform was evaporated. Next, 0.5 or 0.2 mL of water was added, and sonication was carried out for 10 min. After centrifugation at 30,000g for 5 min, the precipitates were

discarded. Finally, DOX@HABN was prepared after dialysis of the supernatant against water for 3 h using Spectra/Por 2 RC Dialysis Membrane Tubing (12,000 to 14,000 Dalton MWCO, Spectrum). To prepare DOX@HABN for in vivo studies, 4 mg of DOX, 4 mg of HA-BR, 4 mL of chloroform, and 0.2 mL of water were used. The amount of DOX loaded in HABN was quantified by HPLC (Agilent 1260, Agilent Technologies). Encapsulation efficiency and drug loading efficiency were calculated according to the following equations: Encapsulation efficiency (%) = (weight of drug in particles/weight of drug added initially) \times 100.

Drug loading percentage (%) = [weight of drug in particles/(weight of drug in particles + weight of HA-BR added initially)] \times 100.

The size and zeta potential of the nanoparticles were obtained using a Nanosizer ZS90 (Malvern Instruments). Their morphology was examined using TEM (JEM-2100F, Jeol). The resulting nanoparticles were diluted in PBS or culture medium for in vitro and in vivo experiments.

ROS Responsiveness of DOX@HABN

For this, 100 μ L of 200 mM 2,2'-azobis (2-methylpropionamide) dihydrochloride (AAPH, Alfa Aesar) was added to 100 μ L of DOX@HABN (10% DOX loading percentage, 10 μ M of DOX; 6.4 μ M of HABN). The decomposition of AAPH produces molecular nitrogen and 2-carbon radicals.³⁵ The carbon radicals may combine to produce stable products or react with molecular oxygen to give peroxy radicals. The half-life of AAPH is about 175 h (37°C at neutral pH), with a constant rate of free radical generation (< μ M/s) during the first several hours in solution. The reaction was monitored every 15 seconds for 1.5 h at 37°C by measuring the absorbance at 450 nm using a microplate reader (Twinfinite 200 PRO, Tecan). The size of HABN upon exposure to ROS at 37°C was also measured at predetermined times (0 h, 1.5 h) using dynamic light scattering (DLS).

Drug Release from HA-BR Upon ROS Exposure

The drug release profile was measured by exposing DOX@HABN (10% DOX loading percentage) to 100 mM AAPH at 37°C. Briefly, 200 μ L of DOX@HABN (10 μ M of DOX; 6.4 μ M of HABN) was mixed with 200 μ L of 100 mM AAPH and incubated for the designated time points (5, 15, 30, 45, and 60 min). Then, the released DOX was removed by dialysis against water for 2 h. The amount of remaining DOX in HABN was quantified by measuring fluorescence with an excitation wavelength of 480 nm and an emission wavelength of 580 nm using a microplate reader (Twinfinite 200 PRO, Tecan).

Cell Culture

HeLa, HepG2, and SK-OV-3 cells were obtained from the American Type Culture Collection (ATCC). The cells were cultured in RPMI-1640 medium (Welgene) containing 10% (v/v) heat-inactivated fetal bovine serum (FBS, Thermo Fisher) and penicillin/streptomycin (100 IU/mL) in a humidified 5% CO₂ atmosphere at 37°C.

Measurement of Intracellular ROS

HeLa, HepG2, and SK-OV-3 cells were plated in 96-well plates (3×10^4 cells per well) and incubated at 37°C for 4 h. The medium was removed, and 30 μ M of 2',7'-dichlorodihydrofluorescein diacetate (DCF-DA, Alfa Aesar) or 100 μ L of fresh medium was added to each well and incubated at 37°C for 1 h. After washing with PBS once, adherent cells were lysed with 100 μ L of RIPA buffer (RIPA cell lysis buffer with EDTA, Alfa Aesar), and the fluorescence intensities of DCF (excitation wavelength of 480 nm and emission wavelength of 525 nm) were measured immediately using a microplate reader (Twinfinite 200 PRO, Tecan).

Measurement of Extracellular ROS

HeLa, HepG2, and SK-OV-3 cells were plated in 96-well plates (3×10^4 cells per well) and incubated at 37°C for 24 h. The cell culture medium was transferred to a fresh 96-well plate, and then 30 μ M of DCF-DA or fresh medium was added to each well and incubated at 37°C for 1 h. The fluorescence intensities of DCF (excitation wavelength of 480 nm

and emission wavelength of 525 nm) were measured immediately using a microplate reader (Twinfinite 200 PRO, Tecan).

ROS Responsiveness of HABN

HeLa cells, HepG2 cells, and SK-OV-3 cells were plated in 96-well plates (5×10^3 cells per well) for 24 h at 37°C. After the medium was removed, cells were treated with 1 mg/mL of HABN for 0.01, 0.5, 1, or 2 h. Next, 100 μ L of the supernatant was diluted in PBS, and the size of the nanoparticles was measured using a Nanosizer ZS90 (Malvern Instruments).

In vitro Confocal Microscopy

HeLa, HepG2, or SK-OV-3 cells were seeded on coverslips in 24-well plates (1×10^4 cells per well). After incubation for 2 d at 37°C, the cells were treated with anti-CD44 antibody conjugated with FITC (5 μ g/mL, BioLegend), HABN-Cy5.5 (15 μ g/mL), free DOX (10 μ M), DOX@HABN (10 μ M of DOX; 6.4 μ M of HABN), or control culture medium at 37°C for 1 h. For a competition study, 5 mg of HA was applied to the cells overnight before nanoparticle treatment. The cells were fixed with 4% paraformaldehyde (Thermo Fisher) for 5 min, counter-stained with Hoechst 33,342 (Life Technologies Corporation) for 10 min, and analyzed using confocal laser scanning microscopy (Nikon A1R).

CCK-8 Assay

HeLa, HepG2, and SK-OV-3 cells were cultured in 96-well plates (4×10^3 cells per well) for 24 h at 37°C. After the medium was removed, cells were treated with different concentrations of free DOX, HABN, DOX@HABN (DOX 0.1, 0.5, 1, 5 μ M), or control fresh medium for 30 min at 37°C and then further incubated for 2 d at 37°C. After removing the medium, 100 μ L of fresh culture medium containing 10 μ L of CCK-8 (Dojindo Molecular Technologies, Inc.) was added for 1 h at 37°C, and the absorbance was measured at 450 nm using a microplate reader (Twinfinite 200 PRO, Tecan).

Animals

Animals were cared for following local guidelines. All work performed on animals was in accordance with and approved by the Institutional Animal Care and Use Committee (IACUC) at Ewha Womans University (EWA IACUC 21-068-4). The guidelines of Ewha Womans University comply with the National Research Council's Guide for the Care and the Use of Laboratory Animals. All animals were obtained from Laonbio as mixed littermates and were housed under pathogen-free conditions in the animal facility at Ewha Womans University. The investigators were not blinded to allocation and outcome assessment except in sections that specified a blind assessment.

In vivo Imaging System (IVIS) Imaging

Six-week-old female Balb/c nude mice were inoculated subcutaneously with 4×10^6 HeLa cells. When the tumor volumes reached 1000 mm³, 20 mg/kg of HABN-Cy5.5 (containing 0.1 mg/kg of Cy5.5) with or without 2 h pre-treatment of free HA (200 mg/kg) was injected intravenously via the tail vein. After 24 h, the mice were sacrificed, and the major organs (colon, kidney, liver, spleen, lung, and heart) were collected. Fluorescence intensities in the major organs from each group were determined using the Xenogen Lumina IVIS with a Cy5.5 filter channel and an exposure time of 5 s. The relative tumor targeting index (RTTI) was calculated according to the following formula: $RTTI = ROI_t / ROI_l$ where ROI_t and ROI_l are the average fluorescence intensity of the tumor and liver, respectively.

In vivo Tumor Study

Six-week-old female Balb/c nude mice were inoculated subcutaneously with 4×10^6 HeLa cells. When the tumor volumes reached at least 50 mm³ (day 0) and injected IV five times with DOX (4 mg/kg), HABN (40 mg/kg), DOX@HABN (4 mg/kg of DOX; 40 mg/kg of DOX), DOX@PEG-BN (4 mg/kg of DOX; 40 mg/kg of PEG-BR), or a PBS control on predetermined days (days 0, 3, 6, 9, and 12). Tumor growth and body weights were checked on predetermined days, and the tumor volume was calculated by the following equation: tumor volume = (length \times width²)/2. The percentage of tumor growth inhibition on the final day was calculated as [(TvolControl - TvolTreatment)/

$Tvol[Control] \times 100$, where $Tvol$ is the final tumor volume minus the initial tumor volume. Mice were sacrificed 34 d after the first treatment, and then the tumors were collected. Apoptotic cells in the tumor sections were detected by using a terminal deoxynucleotidyl transferase dUTP nick-end labeling (TUNEL) assay according to the manufacturer's protocol.

Statistical Analysis

All experiments were performed at least twice with duplicate repeated measures. The results are expressed as means \pm s.e.m. A one-way or two-way analysis of variance (ANOVA) followed by Tukey's honestly significant difference (HSD) multiple comparison post hoc test was used to test the differences among groups. The data were approximately normally distributed, and the variance was similar between the groups. Experiments were repeated multiple times as independent experiments, as indicated in the figure captions. A complete dataset from one representative, independent experiment is shown in each figure. No samples were excluded from the analysis. Statistical significance is indicated as $P < 0.05$. GraphPad Prism v.8.0 (GraphPad Software) was used for statistical analyses.

Results

Preparation of DOX-Loaded HABN (DOX@HABN)

First, HA-BR was synthesized by conjugating HA and pre-prepared amino-ethylene BR through simple amide conjugation ([Supplementary Figure 1](#)). The amount of BR conjugated with each 100 kDa HA molecule was quantified by UV/Vis spectroscopy with an average conjugation density of almost 4 molecules per HA molecule ([Supplementary Figure 2a](#)). In addition, we compared the solubility of HA-BR with free BR. Although BR was insoluble in water, the HA-BR conjugates were easily dispersed in an aqueous buffer ([Supplementary Figure 2b](#)), indicating that the solubility of BR was improved remarkably by conjugation with hydrophilic HA.

To prepare hydrophobic DOX, protonated DOX·HCl was deprotonated under basic conditions with an excess amount of TEA. DOX was then loaded into HABN with a nearly 20% encapsulation efficiency and a maximum loading percentage of almost 10% through simple formation and rehydration ([Figure 1](#) and [Supplementary Figure 3a](#) and [b](#)). The TEM images and DLS measurements revealed that HABN encapsulating DOX (DOX@HABN) comprised spherical-shaped nanoparticles with a diameter of 80 ± 6 nm and a hydrodynamic size and zeta potential value of 131.4 ± 4 nm and -7.10 ± 5 mV, respectively ([Supplementary Figure 3c](#) and [d](#)).

DOX@HABN Selectively Targets Cell Lines Overexpressing CD44

HA is well-known for its ability to target CD44 molecules on the surface of various cells, including immune and cancer cells, through specific HA-CD44 interactions.^{36,37} Therefore, it is expected that HABN also possesses CD44-targeting ability. Before evaluating the ability and efficacy of DOX@HABN, we screened numerous cancer cell lines to identify those with significantly higher CD44 levels. Confocal analysis showed that the HeLa (cervical adenocarcinoma) and SK-OV-3 (ovarian adenocarcinoma) cell lines had high levels of CD44, whereas low levels of CD44 were observed in the HepG2 (hepatocellular carcinoma) cell line ([Figure 2a](#)). To confirm the ability of HABN to target CD44-overexpressing cancer cell lines, DOX@HABN or HABN-Cy5.5 were added to HeLa and SK-OV-3 cells, which are CD44-overexpressing cancer cell lines, and HepG2 cells, which are CD44-negative hepatocyte cells. Although the fluorescence intensities of HABN-Cy5.5 and DOX in DOX@HABN were strong in HeLa and SK-OV-3 cells, minimal signals were observed in HepG2 cells ([Figure 2b](#) and [c](#)). Furthermore, treatment of HeLa cells with an excess of free HA before HABN-Cy5.5 treatment significantly decreased HABN-Cy5.5 intensities ([Figure 2d](#)). These results suggest that HABN specifically targets CD44-overexpressed cancer cells, probably due to specific CD44-HA interactions.

DOX@HABN Releases DOX in Response to ROS

On exposure to ROS, hydrophobic BR becomes hydrophilic biliverdin and BR oxidative products, which increases its water solubility.³⁸ We investigated whether ROS exposure could cause rapid disruption of the nanostructures in DOX@HABN due to solubility changes in the BR core, leading to the release of DOX. When exposed to 100 mM of

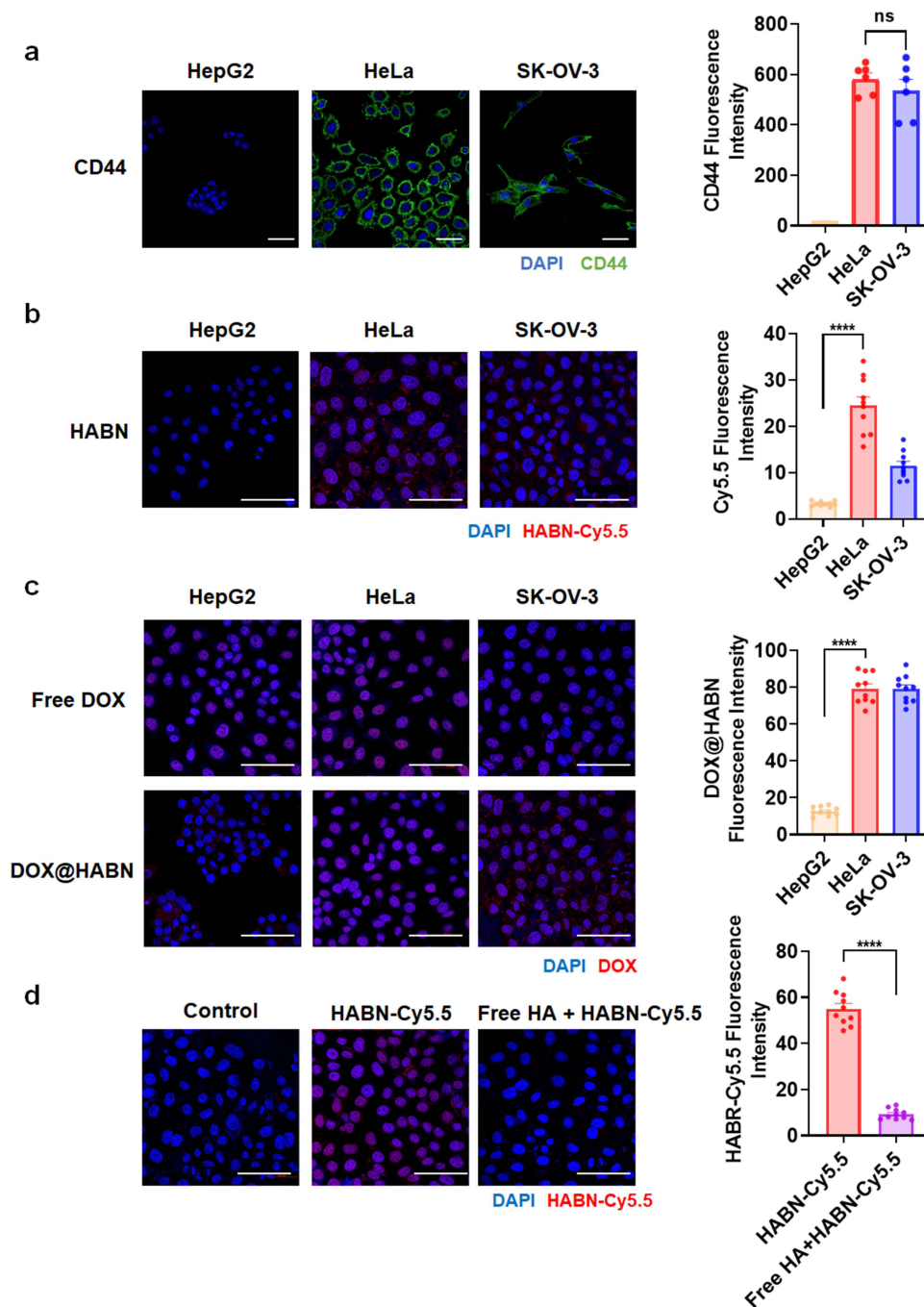


Figure 2 DOX@HABN selectivity targets CD44-overexpressing cell lines. Confocal microscopy images of HeLa, HepG2, and SK-OV-3 cells incubated with (a) anti-CD44 conjugated antibody (5 $\mu\text{g}/\text{mL}$) for 1 h, (b) HABN-Cy5.5 (15 $\mu\text{g}/\text{mL}$), or (c) free doxorubicin (DOX, 10 μM) and DOX@HABN (10 μM of DOX; 0.2 mg/mL of HABN) for 1 h. (d) Confocal microscopic images of HeLa cells treated with DOX@HABN (10 μM of DOX; 0.2 mg/mL of HABN) for 1 h, with or without 1 h pre-treatment with free HA (5 mg/mL). Scale bars, 50 μm . Data are presented as mean \pm s.e.m. **** $p < 0.0001$, analyzed by one-way ANOVA with Tukey's HSD multiple comparison post hoc test.

AAPH, the BR core was rapidly decomposed within two and a half hours, resulting in the disassembly of nanostructures in DOX@HABN (Figure 3a, b and Supplementary Figure 4). Consistent with these results, nearly 100% of DOX was released within 50 min when exposed to ROS, while no drug was released in the absence of ROS exposure (Figure 3c). In consideration that oxidative stress occurs at higher levels in cancer cells and the TME compared to normal tissue,³⁹ we screened three cell lines (HeLa, SK-OV3, and HepG2) using the ROS-detection dye, DCF-DA, to determine which cell lines had higher levels of ROS both intracellularly and extracellularly. The results showed that both intracellular and

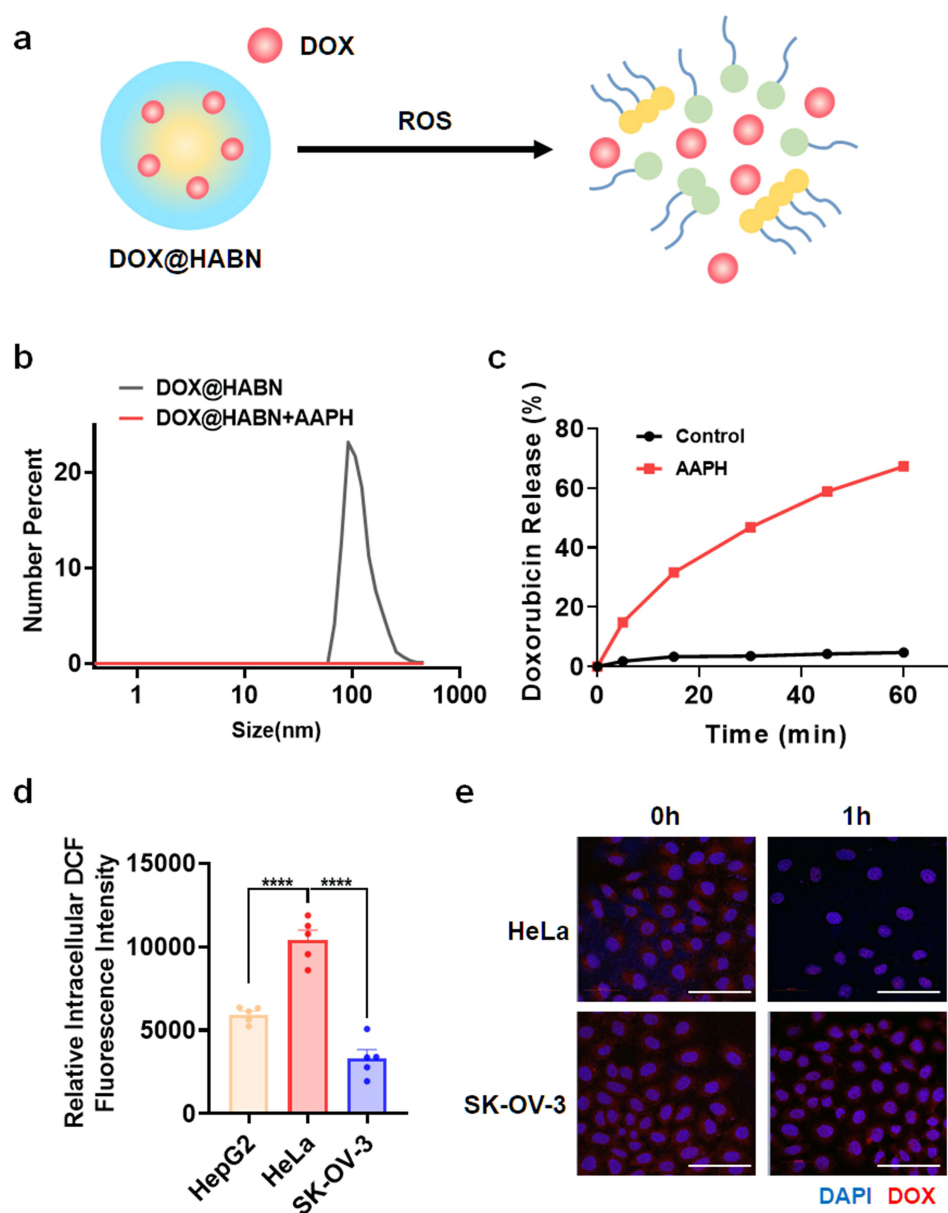


Figure 3 DOX@HABN releases DOX in response to ROS. (a) A scheme for the disassembly of DOX@HABN releasing DOX in response to ROS. (b) Change in the size of HABN induced by the peroxy radical generator, AAPH, at 37°C. (c) DOX release from DOX@HABN (10 μ M of DOX; 0.2 mg/mL of HABN) in the absence and presence of peroxy radical generator, AAPH (100 mM), at 37°C. (d) Comparison of the correlation of ROS levels (determined DCF-DA dye) with fluorescence intensities of HeLa, HepG2, and SK-OV-3 cells. (e) Confocal microscopy images of HeLa cells and SK-OV-3 cells treated with DOX@HABN (10 μ M; 0.2 mg/mL of HABN) with or without 1 h post-incubation with cell culture medium. Scale bars, 50 μ m. Data are presented as mean \pm s.e.m. **** P < 0.0001, analyzed by one-way ANOVA with Tukey's HSD multiple comparison post hoc test.

extracellular ROS levels in HeLa cells are much higher than in HepG2 and SK-OV3 cells (Figure 3d and Supplementary Figure 5), suggesting that CD44-overexpressing/ROS-overproducing HeLa cells are suitable for investigating the therapeutic efficacy of DOX@HABN. After DOX@HABN treatment DOX was much faster localized in the nucleus of HeLa cells than of SK-OV-3 cells, probably due to the rapid ROS-mediated disruption of the HABN structure (Figure 3e). Moreover, nanoparticle sizes significantly decreased in the extracellular regions (cell culture medium) of HeLa cells, but only minor size changes were observed in the extracellular regions of HepG2 cells. Both results are consistent with the intracellular and extracellular ROS results. These findings suggest that either TME ROS or cytosolic ROS can lead to nanoparticle disassembly and rapid drug release.

DOX@HABN Shows Synergistic Anti-Cancer Activity in vitro

Given the potential of BR as an anti-cancer agent,²⁵ we investigated whether DOX@HABN shows synergistic anti-cancer activity of loaded DOX and the nanocarrier. The cell viability analysis showed that DOX@HABN had significantly higher anti-cancer activity than HABN and DOX alone in HeLa cells, indicating the synergistic combined activity of the released DOX and HABN cargo (Figure 4a). Notably, as shown in Figure 4a, HABN itself demonstrated anti-cancer efficacy in HeLa cells. In contrast, DOX@HABN demonstrated minimal toxicity in HepG2 cells with low CD44/low ROS expression (normal human hepatocytes) (Supplementary Figure 6). Moreover, treatment with free HA before DOX@HABN treatment significantly decreased the in vitro therapeutic efficacy of DOX@HABN in HeLa cells, further emphasizing the important role of CD44-mediated DOX@HABN uptake in the synergistic therapeutic activity (Figure 4b).

DOX@HABN Exhibits Enhanced in vivo Targeting Ability Toward CD44-Overexpressing HeLa Tumors

Next, to investigate whether HABN could target CD44-overexpressing ROS-overproducing HeLa cell tumors in vivo, IVIS images were acquired after HABN-Cy5.5 with or without free HA pre-treatment was intravenously administered into HeLa tumor-bearing mice. IVIS imaging of the major organs and tumors revealed that most of the fluorescence intensity of HABN-Cy5.5 was observed in the tumor, yielding a remarkably high RTTI (a ratio of the average fluorescence intensity between the tumor and the liver) of 7.55 (Figure 5). Most remaining signals of HABN-Cy5.5 were observed in the kidney, a major safe excretion route, while a few signals were detected in the liver and other major organs (Figure 5). Notably, the signal intensity of HABN-Cy5.5 in the tumors of mice pre-treated with free HA was significantly lower than that of mice treated with HABN-Cy5.5 alone (Figure 5). These results indicate that HABN has remarkably high tumor-targeting ability in vivo owing to both nanoparticle-mediated enhanced permeability and retention (EPR) effects and HA shell-mediated active targeting effects.

DOX@HABN Exerts Improved Anti-Cancer Activity in vivo

Based on the findings that DOX@HABN demonstrates enhanced anti-cancer activity in vitro and tumor-targeting ability in vitro and in vivo, we hypothesized that DOX@HABN could also exhibit improved synergistic anti-cancer activity in vivo. To test this hypothesis, we compared the therapeutic efficacy of intravenously administered DOX@HABN with those of free DOX, HABN alone, and DOX@PEGylated-BR nanoparticles (PEG-BN), a non-targeted version of BR nanoparticles, in HeLa tumor-bearing mice (Figure 6a). HABN alone inhibited tumor growth by $23.89 \pm 3.19\%$ compared to the control group, suggesting that HABN itself has intrinsic anti-cancer activity, probably owing to its

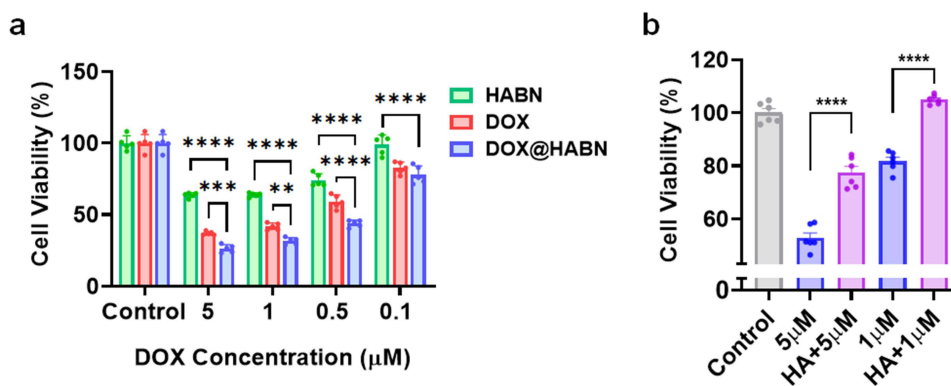


Figure 4 DOX@HABN exerts synergistic anti-cancer activity in vitro. (a) Cell viability of HeLa cells treated with different concentrations of DOX@HABN (10% DOX loading percentage), DOX (equivalent to the concentrations of DOX in DOX@HABN), and HABN (equivalent to the concentrations of HABN in DOX@HABN) for 30 min, followed by further incubation for 48 h. (b) Viability of HeLa cells pre-treated with free HA (5 mg/mL) for 24 h and then treated with different concentrations of DOX@HABN for 2 h. Data are presented as mean \pm s.e.m. from a representative experiment. ** $P < 0.01$, *** $P < 0.001$, **** $P < 0.0001$, analyzed by one-way ANOVA with Tukey's HSD multiple comparison post hoc test.

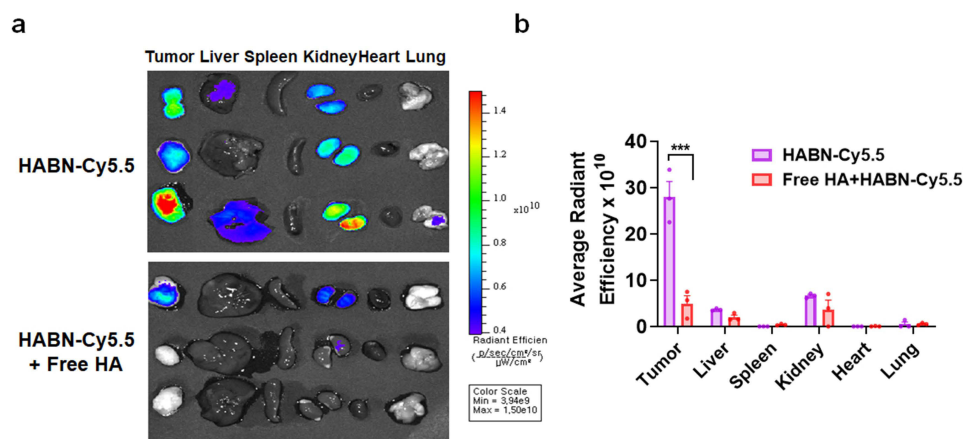


Figure 5 DOX@HABN shows enhanced in vivo tumor-targeting ability. (a and b) Balb/c nude mice bearing HeLa tumor were IV administered with HABN-Cy5.5 (containing 0.1 mg/kg of Cy5.5) with or without free HA pre-treatment (200 mg/kg). After 24 h, major organs (tumor, liver, spleen, kidney, heart, and lung) were imaged by an in vivo imaging system (IVIS), (a) and Cy5.5 fluorescence signal was quantified (b). Data are presented as mean \pm s.e.m. from a representative experiment. *** $P < 0.001$, analyzed by two-tailed unpaired Student's test.

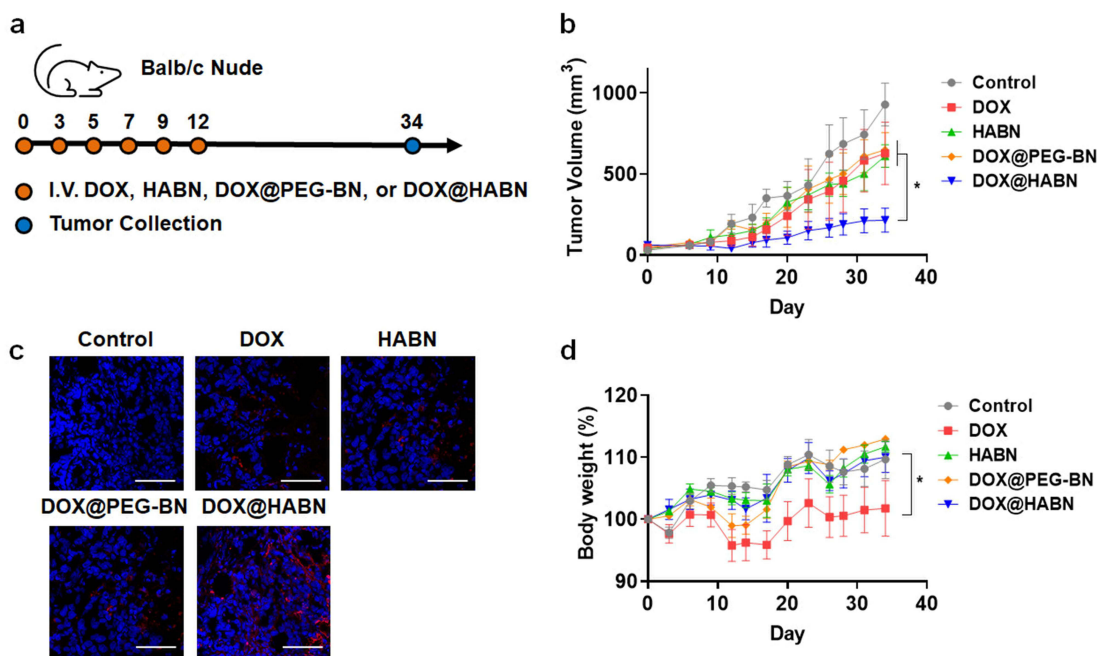


Figure 6 DOX@HABN exerts synergistic anti-cancer activity in vivo. (a and b) Balb/c nude mice bearing HeLa tumor (size $>50 \text{ mm}^2$) were IV administered with PBS (control), free DOX (4 mg/kg), HABN (40 mg/kg), DOX@HABN (DOX: 4 mg/kg; HABN: 40 mg/kg), or DOX@PEG-BN (DOX: 4 mg/kg; HABN: 40 mg/kg). Tumor volumes (b) were measured on predetermined days. (c), Tumor tissue from HeLa tumor-bearing mice treated as shown was processed using a TUNEL assay and visualized by confocal microscopy. Scale bars, 10 μm . (d), Body weight measured on predetermined days. Data are presented as mean \pm s.e.m. from a representative experiment ($n = 5$). * $P < 0.05$, analyzed by one-way ANOVA with Tukey's HSD multiple comparison post hoc test.

BR core (Figure 6b). Notably, DOX@HABN demonstrated significantly greater anti-tumor efficacy, inhibiting tumor growth by about 83.8% compared to free DOX (35.3% inhibition) and HABN alone (36.3% inhibition) (Figure 6b), suggesting that DOX@HABN exhibited synergistic anti-cancer activity. In contrast, DOX@PEG-BN showed significantly lower therapeutic efficacy (30% inhibition) compared to DOX@HABN (83.8% inhibition), probably due to the lack of HA-mediated targeting ability (Figure 6b) which is correlated with the decreased targeting ability of HABN-Cy5.5 against the tumors of mice pre-treated with free HA (Figure 5). Furthermore, TUNEL assays demonstrated synergistic and greater anti-cancer activity of DOX@HABN compared to other groups (Figure 6c). Moreover, while DOX caused systemic toxicity, no overt toxicity was observed in mice treated with DOX@HABN (Figure 6d and [Supplementary](#)

[Figure 6](#)). These results highlight the efficacy and safety of DOX@HABN and demonstrate that the potent anti-cancer activity of DOX@HABN is due to the combined synergistic activity of the HA shell and BR core.

Discussion

We report the development of DOX@HABN, a nanomedicine specifically designed to target cancer cells and respond to TME ROS, thereby enhancing the specificity of targeted cancer therapy ([Figure 1](#)). DOX@HABN, with a size of 100 nm, was conveniently prepared by using a simple one-step film layer process. The ROS-responsive disruption exhibited by DOX@HABN leads to the release of drugs owing to the ROS responsiveness of the BR core ([Figure 3a–c](#)).^{25,38} DOX@HABN showed specific uptake in CD44-overexpressing HeLa and SK-OV3 cells via the HA shell and CD44 interactions on the cancer cell surface, whereas minimal uptake was observed in CD44-negative HepG2 cells ([Figure 2](#)).^{36,37} Once taken up by the cells, DOX loaded in HABN was rapidly localized to the nucleus in HeLa cells with higher levels of ROS than in SKOV3 cells, probably caused by the ROS-mediated release of DOX ([Figure 3d and e](#)). Furthermore, DOX@HABN exhibited synergistic anti-cancer activity in CD44-overexpressing/ROS-overproducing HeLa cells while demonstrating minimal toxicity in HepG2 cells with low CD44/low ROS expression ([Figure 4 and Supplementary Figure 6](#)). The intravenous injection of DOX@HABN accumulated preferentially in HeLa tumors, presumably through both passive EPR effects and specific active interactions with CD44, a receptor of the HA shell ([Figure 5](#)).²⁸ Surprisingly, compared to the other conventional nanoparticles, which are mainly taken up by immune cells (eg macrophages) in the liver and the spleen, resulting in a low RTTI of below 1,^{40,41} most of the HABN localized to tumors, demonstrating a remarkably high RTTI of 7.55, which is probably due to the inherent TME ROS and CD44-targeting ability of HABN. Interestingly, HABN might be excreted through the kidney which is a major safe elimination route in drug delivery, with limited localization into the liver, where conventional nanoparticles tend to accumulate.⁴² Based on that information, we hypothesized that DOX@HABN would exhibit potent anti-cancer activity in vivo while demonstrating minimal toxicity in mice. In line with our hypothesis, DOX@HABN exhibited potent anti-cancer activity in HeLa tumors in vivo, resulting from the synergistic combined activity of the HA shell and the BR core with a good safety profile ([Figures 6](#)). Our findings highlight DOX@HABN as a promising drug delivery system that targets TME ROS of CD44-overexpressing tumors, leading to significant enhancement of tumor targeting and anti-tumor potency/efficacy. The following three sequential mechanisms probably contribute to the enhanced tumor targeting and anti-cancer activity: 1) substantial accumulation of DOX@HABN within tumor tissue due to both passive EPR effects of HABN and CD44-targeting ability of the HA shell, 2) rapid disassembly of the DOX@HABN into nanoparticle fragments by ROS-mediated solubility changes of the BR core, releasing DOX into the tumor tissue, and 3) penetration of both the fragments and the released DOX deep into the tumor, potentially reaching cancer cells and exhibiting synergistic anti-cancer activity.

In conclusion, whereas the ROS-responsive nanomedicines developed to date usually comprise *de novo*-synthesized artificial materials with slow ROS responsiveness, our work presents a promising simple drug delivery system. The system, based on HABN and composed of naturally occurring biocompatible and biodegradable material (HA and BR), demonstrates rapid drug release in response to various endogenous ROS and exerts intrinsic anti-cancer activity. Furthermore, HABN demonstrated a remarkably high RTTI and possesses renal-clearance properties, although the exact mechanisms should be further investigated. These characteristics strengthen the potential for the clinical translational of the system. Overall, our findings suggest that HABN holds great potential as a TME ROS-responsive nanomedicine for targeted cancer therapy against various tumors.

Abbreviations

TME, Tumor microenvironment; ROS, Reactive oxygen species; DOX, Doxorubicin; HA, Hyaluronic acid; BR, Bilirubin; AE-BR, Aminoethylene-bilirubin conjugate; HA-BR, Hyaluronic acid-bilirubin conjugate; HABN, Hyaluronic acid-bilirubin nanoparticles; DOX@HABN, Doxorubicin-loaded hyaluronic acid-bilirubin nanoparticles; PEG-BR, PEGylated bilirubin conjugate; PEG-BN, PEGylated bilirubin nanoparticles; DOX@PEG-BN, Doxorubicin-loaded PEGylated Bilirubin Nanoparticles.

Data Sharing Statement

The authors declare that data supporting the findings of this study are available within the article and its [Supplementary Information files](#). All relevant data can be provided by the corresponding author upon reasonable request.

Ethics Approval and Informed Consent

All work performed on animals was in accordance with and approved by the Institutional Animal Care and Use Committee (IACUC) at Ewha Womans University (EWAH IACUC 21-068-4). The guidelines of Ewha Womans University comply with the National Research Council's Guide for the Care and the Use of Laboratory Animals.

Acknowledgments

The authors would like to thank the Ewha Drug Development Research Core Center and the Ewha Fluorescence Core Imaging Center for UV/Vis spectroscopy analysis, Zetasizer analysis, HPLC analysis, IVIS analysis, and Confocal analysis. This paper is based on the thesis of Seonju Lee. It has been published on the institutional website: <https://dspace.ewha.ac.kr/handle/2015.oak/264236>.

Author Contributions

All authors made a significant contribution to the work reported, whether that is in the conception, study design, execution, acquisition of data, analysis and interpretation, or in all these areas; took part in drafting, revising or critically reviewing the article; gave final approval of the version to be published; have agreed on the journal to which the article has been submitted; and agree to be accountable for all aspects of the work.

Funding

The Basic Science Research Program through the National Research Foundation of Korea (NRF) funded by the Ministry of Education supported this research (2022M3H4A1A03067401). This research was also supported by a grant of the Korea Health Technology R&D Project through the Korea Health Industry Development Institute (KHIDI), funded by the Ministry of Health & Welfare, Republic of Korea (RS-2023-00265981). A Korea Basic Science Institute (National Research Facilities and Equipment Center) grant funded by the Ministry of Education supported this research (2023R1A6C103A026).

Disclosure

Prof. Dr. Yonghyun Lee reports a licensed bilirubin nanoparticle patent (US11904019B2) used for preparation of methods. The authors have no other competing interests to declare in this work.

References

1. Binnewies M, Roberts EW, Kersten K, et al. Understanding the tumor immune microenvironment (TIME) for effective therapy. *Nat Med.* 2018;24(5):541–550. doi:10.1038/s41591-018-0014-x
2. Quail DF, Joyce JA. Microenvironmental regulation of tumor progression and metastasis. *Nat Med.* 2013;19(11):1423–1437. doi:10.1038/nm.3394
3. Pitt JM, Marabelle A, Eggermont A, Soria JC, Kroemer G, Zitvogel L. Targeting the tumor microenvironment: removing obstruction to anticancer immune responses and immunotherapy. *Ann Oncol.* 2016;27(8):1482–1492. doi:10.1093/annonc/mdw168
4. Perillo B, Di Donato M, Pezone A, et al. ROS in cancer therapy: the bright side of the moon. *Exp Mol Med.* 2020;52(2):192–203. doi:10.1038/s12276-020-0384-2
5. Boedtker E, Pedersen SF. The acidic tumor microenvironment as a driver of cancer. *Annu Rev Physiol.* 2020;82:103–126. doi:10.1146/annurev-physiol-021119-034627
6. Khrantsov VV, Gillies RJ. Janus-faced tumor microenvironment and redox. *Antioxid Redox Sign.* 2014;21(5):723–729. doi:10.1089/ars.2014.5864
7. Hanahan D, Coussens LM. Accessories to the crime: functions of cells recruited to the tumor microenvironment. *Cancer Cell.* 2012;21(3):309–322. doi:10.1016/j.ccr.2012.02.022
8. Shinn J, Kwon N, Lee SA, Lee Y. Smart pH-responsive nanomedicines for disease therapy. *J Pharm Invest.* 2022;52(4):427–441. doi:10.1007/s40005-022-00573-z
9. Sahu BP, Baishya R, Hatiboruah JL, Laloo D, Biswas N. A comprehensive review on different approaches for tumor targeting using nanocarriers and recent developments with special focus on multifunctional approaches. *J Pharm Invest.* 2022;52(5):539–585. doi:10.1007/s40005-022-00583-x
10. Mitchell MJ, Billingsley MM, Haley RM, Wechsler ME, Peppas NA, Langer R. Engineering precision nanoparticles for drug delivery. *Nat Rev Drug Discov.* 2021;20(2):101–124. doi:10.1038/s41573-020-0090-8

11. Wang J, Li Y, Nie G. Multifunctional biomolecule nanostructures for cancer therapy. *Nat Rev Mater.* 2021;6(9):766–783. doi:10.1038/s41578-021-00315-x
12. Peng S, Xiao F, Chen M, Gao H. Tumor-microenvironment-responsive nanomedicine for enhanced cancer immunotherapy. *Adv Sci.* 2022;9(1):e2103836. doi:10.1002/advs.202103836
13. Yang B, Chen Y, Shi J. Reactive Oxygen Species (ROS)-based nanomedicine. *Chem Rev.* 2019;119(8):4881–4985. doi:10.1021/acs.chemrev.8b00626
14. Luo L, Xu F, Peng H, et al. Stimuli-responsive polymeric prodrug-based nanomedicine delivering nifuroxazide and doxorubicin against primary breast cancer and pulmonary metastasis. *J Control Release.* 2020;318:124–135. doi:10.1016/j.jconrel.2019.12.017
15. Mura S, Nicolas J, Couvreur P. Stimuli-responsive nanocarriers for drug delivery. *Nature Mater.* 2013;12(11):991–1003. doi:10.1038/Nmat3776
16. Zhang C, Wang X, Du J, Gu Z, Zhao Y. Reactive oxygen species-regulating strategies based on nanomaterials for disease treatment. *Adv Sci.* 2021;8(3):2002797. doi:10.1002/advs.202002797
17. Fu X, Hosta-Rigau L, Chandrawati R, Cui JW. Multi-stimuli-responsive polymer particles, films, and hydrogels for drug delivery. *Chem-Us.* 2018;4(9):2084–2107. doi:10.1016/j.chempr.2018.07.002
18. Saravanakumar G, Kim J, Kim WJ. Reactive-oxygen-species-responsive drug delivery systems: promises and challenges. *Adv Sci.* 2017;4(1):1600124. doi:10.1002/advs.201600124
19. Patra JK, Das G, Fraceto LF, et al. Nano based drug delivery systems: recent developments and future prospects. *J Nanobiotechnology.* 2018;16(1):71. doi:10.1186/s12951-018-0392-8
20. Dang Y, Guan J. Nanoparticle-based drug delivery systems for cancer therapy. *Smart Mater Med.* 2020;1:10–19. doi:10.1016/j.smaim.2020.04.001
21. He H, Liu L, Morin EE, Liu M, Schwendeman A. Survey of clinical translation of cancer nanomedicines-lessons learned from successes and failures. *Acc Chem Res.* 2019;52(9):2445–2461. doi:10.1021/acs.accounts.9b00228
22. Cheng Z, Li M, Dey R, Chen Y. Nanomaterials for cancer therapy: current progress and perspectives. *J Hematol Oncol.* 2021;14(1):85. doi:10.1186/s13045-021-01096-0
23. Navya PN, Kaphle A, Srinivas SP, Bhargava SK, Rotello VM, Daima HK. Current trends and challenges in cancer management and therapy using designer nanomaterials. *Nano Conver.* 2019;6(1):23. doi:10.1186/s40580-019-0193-2
24. Jansen T, Daiber A. Direct antioxidant properties of bilirubin and biliverdin. is there a role for biliverdin reductase? *Front Pharmacol.* 2012;3:30. doi:10.3389/fphar.2012.00030
25. Sedlak TW, Saleh M, Higginson DS, Paul BD, Juluri KR, Snyder SH. Bilirubin and glutathione have complementary antioxidant and cytoprotective roles. *Proc Natl Acad Sci U S A.* 2009;106(13):5171–5176. doi:10.1073/pnas.0813132106
26. Chen Z, Vong CT, Gao C, et al. Bilirubin nanomedicines for the treatment of reactive oxygen species (ROS)-mediated diseases. *Mol Pharm.* 2020;17(7):2260–2274. doi:10.1021/acs.molpharmaceut.0c00337
27. Lee Y, Shinn J, Xu C, Dobson HE, Neamati N, Moon JJ. Hyaluronic acid-bilirubin nanomedicine-based combination chemoimmunotherapy. *Nat Commun.* 2023;14(1):4771. doi:10.1038/s41467-023-40270-5
28. Zoller M. CD44: can a cancer-initiating cell profit from an abundantly expressed molecule? *Nat Rev Cancer.* 2011;11(4):254–267. doi:10.1038/nrc3023
29. Peach RJ, Hollenbaugh D, Stamenkovic I, Aruffo A. Identification of hyaluronic acid binding sites in the extracellular domain of CD44. *J Cell Biol.* 1993;122(1):257–264. doi:10.1083/jcb.122.1.257
30. Banerji S, Wright AJ, Noble M, et al. Structures of the Cd44-hyaluronan complex provide insight into a fundamental carbohydrate-protein interaction. *Nat Struct Mol Biol.* 2007;14(3):234–239. doi:10.1038/nsmb1201
31. Lee Y, Sugihara K, Gilliland MG, Jon S, Kamada N, Moon JJ. Hyaluronic acid-bilirubin nanomedicine for targeted modulation of dysregulated intestinal barrier, microbiome and immune responses in colitis. *Nat Mater.* 2020;19(1):118–126. doi:10.1038/s41563-019-0462-9
32. Shinn J, Park S, Lee S, et al. Antioxidative hyaluronic acid-bilirubin nanomedicine targeting activated hepatic stellate cells for anti-hepatic-fibrosis therapy. *ACS Nano.* 2024;18(6):4704–4716. doi:10.1021/acsnano.3c06107
33. Lee Y, Lee S, Jon S. Biotinylated bilirubin nanoparticles as a tumor microenvironment-responsive drug delivery system for targeted cancer therapy. *Adv Sci.* 2018;5(6):1800017. doi:10.1002/advs.201800017
34. Lee Y, Lee S, Lee DY, Yu B, Miao W, Jon S. Multistimuli-responsive bilirubin nanoparticles for anticancer therapy. *Angew Chem Int Ed Engl.* 2016;55(36):10676–10680. doi:10.1002/anie.201604858
35. Betigeri S, Thakur A, Raghavan K. Use of 2,2'-Azobis(2-amidinopropane) dihydrochloride as a reagent tool for evaluation of oxidative stability of drugs. *Pharm Res-Dordr.* 2005;22(2):310–317. doi:10.1007/s11095-004-1199-x
36. Heldin P, Karousou E, Bernert B, Porsch H, Nishitsuka K, Skandalis SS. Importance of hyaluronan-CD44 interactions in inflammation and tumorigenesis. *Connect Tissue Res.* 2008;49(3):215–218. doi:10.1080/03008200802143323
37. Negi LM, Talegaonkar S, Jaggi M, Ahmad FJ, Iqbal Z, Khar RK. Role of CD44 in tumour progression and strategies for targeting. *J Drug Target.* 2012;20(7):561–573. doi:10.3109/1061186X.2012.702767
38. Kapitulnik JB. An endogenous product of heme degradation with both cytotoxic and cytoprotective properties. *Mol Pharmacol.* 2004;66(4):773–779. doi:10.1124/mol.104.002832
39. Reczek CR, Chandel NS. The two faces of reactive oxygen species in cancer. *Annu Rev Canc Biol.* 2017;1:79–98. doi:10.1146/annurev-cancerbio-041916-065808
40. Ao H, Wang Z, Lu LK, et al. Enhanced tumor accumulation and therapeutic efficacy of liposomal drugs through over-threshold dosing. *J Nanobiotechnol.* 2022;20(1). doi:10.1186/s12951-022-01349-1
41. Wilhelm S, Tavares AJ, Dai Q, et al. Analysis of nanoparticle delivery to tumours. *Nature Rev Mater.* 2016;1(5):1–2.
42. Baek MJ, Nguyen DT, Kim D, et al. Tailoring renal-clearable zwitterionic cyclodextrin for colorectal cancer-selective drug delivery. *Nat Nanotechnol.* 2023;18(8):945. doi:10.1038/s41565-023-01381-8

International Journal of Nanomedicine

Dovepress

Publish your work in this journal

The International Journal of Nanomedicine is an international, peer-reviewed journal focusing on the application of nanotechnology in diagnostics, therapeutics, and drug delivery systems throughout the biomedical field. This journal is indexed on PubMed Central, MedLine, CAS, SciSearch[®], Current Contents[®]/Clinical Medicine, Journal Citation Reports/Science Edition, EMBase, Scopus and the Elsevier Bibliographic databases. The manuscript management system is completely online and includes a very quick and fair peer-review system, which is all easy to use. Visit <http://www.dovepress.com/testimonials.php> to read real quotes from published authors.

Submit your manuscript here: <https://www.dovepress.com/international-journal-of-nanomedicine-journal>